



CHORUS

This is the accepted manuscript made available via CHORUS. The article has been published as:

Volkov basis for simulation of interaction of strong laser pulses and solids

Daniel Kidd, Cody Covington, Yonghui Li, and Kálmán Varga

Phys. Rev. B **97**, 024303 — Published 9 January 2018

DOI: [10.1103/PhysRevB.97.024303](https://doi.org/10.1103/PhysRevB.97.024303)

Volkov basis for simulation of interaction of strong laser pulses and solids

Daniel Kidd and Cody Covington

Department of Physics and Astronomy, Vanderbilt University, Nashville, Tennessee 37235, USA

Yonghui Li

Department of Physics, School of Science, Tianjin University, Tianjin 300072, China

Kálmán Varga*

Department of Physics and Astronomy, Vanderbilt University, Nashville, Tennessee 37235, USA
(Dated: December 27, 2017)

An efficient and accurate basis comprised of Volkov states is implemented and tested for time-dependent simulations of interactions between strong laser pulses and crystalline solids. The Volkov states are eigenstates of the free electron Hamiltonian in an electromagnetic field and analytically represent the rapidly oscillating time-dependence of the orbitals, allowing **significantly** faster time propagation than conventional approaches. The Volkov approach can be readily implemented in plane wave codes by multiplying the potential energy matrix elements with a simple time-dependent phase factor.

New subfemtosecond pump probe experiments have brought “an era of control of the quantum world” enabling scientists to observe electron dynamics in molecules and solids directly on their natural length (Angstrom) and time (attosecond) scales [1, 2]. The availability of super-intense laser pulses [3, 4] allows for direct control of electric and optical properties of materials. New experimental approaches—for example coherent extreme-ultraviolet pulse production with high harmonics generation [5, 6] and attosecond streaking [7]—lead to enhanced control over lightmatter interactions.

These unprecedented capabilities call for vigorous theoretical and computational studies of the dynamics of laser-matter interactions in the strong field regime. Semi-classical approaches describing the coupled light-field induced interband and intraband dynamics in the framework of the optical Bloch equations are very popular in interpreting experimental results [8–10]. More recently, time-dependent density functional theory (TDDFT) [11] coupled with classical electromagnetic fields has also been used to simulate the effect of laser pulses in electron and nuclear dynamics [12–17].

In this work we introduce the Volkov states as an efficient and accurate basis for time-dependent simulation of interaction between strong laser pulses and solids. To simulate the effect of strong, rapidly oscillating electric fields one needs a very fine time mesh to represent the temporal change of the wave function. The Volkov state, the eigenstate of a free electron in electromagnetic field, absorbs the oscillatory time-dependence in a phase factor and allow for the use of a coarser time grid. Using the TDDFT Hamiltonian description of solids, we will

show that using the Volkov state basis allows for **revisignificantly** faster time propagation than conventional representations.

The Volkov states may be expressed as

$$\phi_{\mathbf{k}}^{\text{V}}(\mathbf{r}, t) = \frac{1}{\sqrt{\Omega}} e^{i\mathbf{k}\cdot\mathbf{r}} e^{-i\Phi^{\mathbf{k}}(t)} = \phi_{\mathbf{k}}^{\text{PW}}(\mathbf{r}) e^{-i\Phi^{\mathbf{k}}(t)}, \quad (1)$$

where $\phi_{\mathbf{k}}^{\text{PW}}(\mathbf{r})$ is a plane wave, Ω is the normalizing volume of the computational space and the time-dependent Volkov phase is described by

$$\Phi^{\mathbf{k}}(t) = \int_0^t \frac{1}{2} [\mathbf{k} + \mathbf{A}(\tau)]^2 d\tau. \quad (2)$$

These states satisfy the time-dependent Schrödinger equation (TDSE) for a free electron subject to an external vector potential, \mathbf{A} :

$$i \frac{\partial}{\partial t} \phi_{\mathbf{k}}^{\text{V}}(\mathbf{r}, t) = H^{\text{V}}(t) \phi_{\mathbf{k}}^{\text{V}}(\mathbf{r}, t), \quad H^{\text{V}}(t) = \frac{1}{2} [\mathbf{p} + \mathbf{A}(t)]^2 \quad (3)$$

(atomic units (a.u.) of $\hbar = m_e = e = 1/4\pi\epsilon_0 = 1$ are used throughout).

Defining the Hamiltonian as

$$H = H^{\text{V}}(t) + V(\mathbf{r}, t) = \frac{1}{2} [\mathbf{p} + \mathbf{A}(t)]^2 + V(\mathbf{r}, t), \quad (4)$$

where $V(\mathbf{r}, t)$ may be the Kohn–Sham potential in TDDFT calculations, the TDSE takes the form

$$i \frac{\partial}{\partial t} \psi(\mathbf{r}, t) = [H^{\text{V}}(t) + V(\mathbf{r}, t)] \psi(\mathbf{r}, t). \quad (5)$$

Using the Volkov states as the basis,

$$\psi(\mathbf{r}, t) = \sum_{\mathbf{k}} c_{\mathbf{k}}(t) \phi_{\mathbf{k}}^{\text{V}}(\mathbf{r}, t), \quad (6)$$

* kalman.varga@vanderbilt.edu

the TDSE, in matrix representation, becomes

$$i\dot{\mathbf{c}}^V(t) = \mathbf{V}^V(t)\mathbf{c}^V(t). \quad (7)$$

Here, the matrix elements of \mathbf{V}^V are defined as

$$V_{\mathbf{k}\mathbf{k}'}^V(t) = \langle \phi_{\mathbf{k}}^V(t) | V(t) | \phi_{\mathbf{k}'}^V(t) \rangle, \quad (8)$$

and the notation of column vector $\mathbf{c}^V = (c_{\mathbf{k}_1}^V(t), c_{\mathbf{k}_2}^V(t), \dots, c_{\mathbf{k}_N}^V(t))$ has been employed. It is useful at this point to compare Eq. (7) to the plane wave representation of the TDSE:

$$i\dot{\mathbf{c}}^{\text{PW}}(t) = \mathbf{H}^{\text{PW}}(t)\mathbf{c}^{\text{PW}}(t) \quad (9)$$

where

$$H_{\mathbf{k}\mathbf{k}'}^{\text{PW}}(t) = \langle \phi_{\mathbf{k}}^{\text{PW}}(t) | H | \phi_{\mathbf{k}'}^{\text{PW}}(t) \rangle. \quad (10)$$

The difference between the two equations is that in the Volkov basis representation the matrix elements of the potential governs the evolution, while in the case of the plane wave representation the driving term is the whole Hamiltonian.

In the Volkov basis representation, the stiff $\frac{1}{2}[\mathbf{p} + \mathbf{A}(t)]^2$ operator is removed from the Hamiltonian and absorbed into the basis as a phase factor. This phase factor is illustrated for a sample external vector potential in Fig. 1. It is shown that this time-dependent behavior of the expansion coefficients occurs on a timescale which may be much shorter than that of the causal vector potential. The advantage of the Volkov expansion, then, is clear as this phase factor may be analytically included rather than numerically propagated.

In the case of a differential equation of the form found in Eqs. (9) and (7),

$$i\dot{\mathbf{c}}(t) = \mathbf{H}(t)\mathbf{c}(t), \quad (11)$$

one may determine a formally exact solution for the expansion coefficients at some desired time, $\mathbf{c}(t)$, as

$$\mathbf{c}(t) = U(t, 0)\mathbf{c}(0), \quad (12)$$

where $U(t, 0)$ is known as the time evolution operator

$$U(t, t_0) = \mathcal{T} \exp \left\{ -i \int_{t_0}^t \mathbf{H}(t') dt' \right\} \quad (13)$$

which includes time-ordering, \mathcal{T} . A common method for approximating this operator is to take discrete small time steps, Δt , which allow the Hamiltonian to remain nearly constant, i.e. $\mathbf{H}(t) \approx \mathbf{H}(t + \Delta t)$. In this way, the integral and time-ordering may be satisfied approximately. One may, thus, rewrite Eq. (12) as

$$\mathbf{c}(t) \approx \left[\prod_{n=0}^{N_t} U_n \right] \mathbf{c}(0), \quad (14)$$

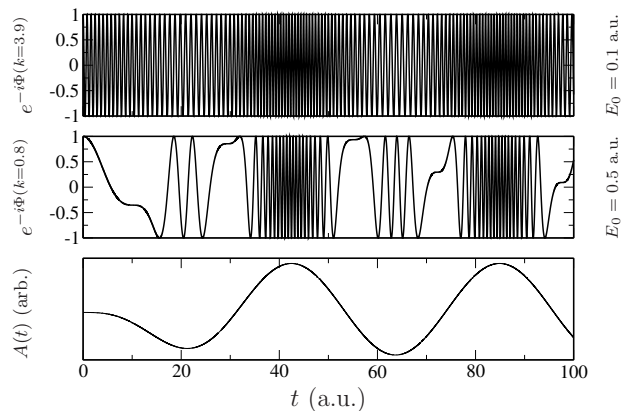


FIG. 1. Time-dependent phase factors at $k = 3.9$ a.u. (top) and $k = 0.8$ a.u. (middle) included in the analytic solution of the TDSE using the Volkov Hamiltonian with electric field amplitudes of $E_0 = 0.1$ a.u. and $E_0 = 0.5$ a.u., respectively. The shape of the vector potential is presented for arbitrary units (bottom).

where

$$U_n = e^{-i\mathbf{H}(t_n)\Delta t}. \quad (15)$$

This matrix exponential may be approximated using popular techniques such as Taylor expansion or the Crank-Nicolson method.

To illuminate the difference between time propagation on the Volkov state and plane wave representations, we present a model calculation of one-electron in a one-dimensional, periodic Mathieu potential, $V(x) = -V_0[1 + \cos(2\pi x/L)]$, subject to an oscillating external electric field in Fig. 2. The parameters of the potential were set to be $V_0 = 0.37$ Hartree and $L = 8$ Bohr. The electric field used followed the form

$$E(t) = \begin{cases} E_0 \sin(\frac{\pi t}{2T_r}) \sin(\omega t), & \text{if } 0 \leq t \leq T_r, \\ E_0 \sin(\omega t), & \text{otherwise,} \end{cases} \quad (16)$$

which provided a vector potential determined by the relationship

$$A(t) = - \int_0^t E(t') dt'. \quad (17)$$

Figures 2a and 2b indicate the oscillatory nature of the expansion coefficients by plotting the metric $\langle \dot{c} \rangle = \int \langle \text{Re} \{ \dot{c}_k \} \rangle_t dk$ for a range of field strengths and frequencies. This metric is related to the time-averaged rate of change of these coefficients over time which is indicative of the difficulty in using Eq. (15) to numerically propagate the wave function.

In this case, where the Hamiltonian is of the form $H^V + V$, the Volkov state expansion is expected to perform best when the frequency, and, thus, the energy, of the external field is high enough so that the perturbation of the Mathieu potential becomes negligible. This is due

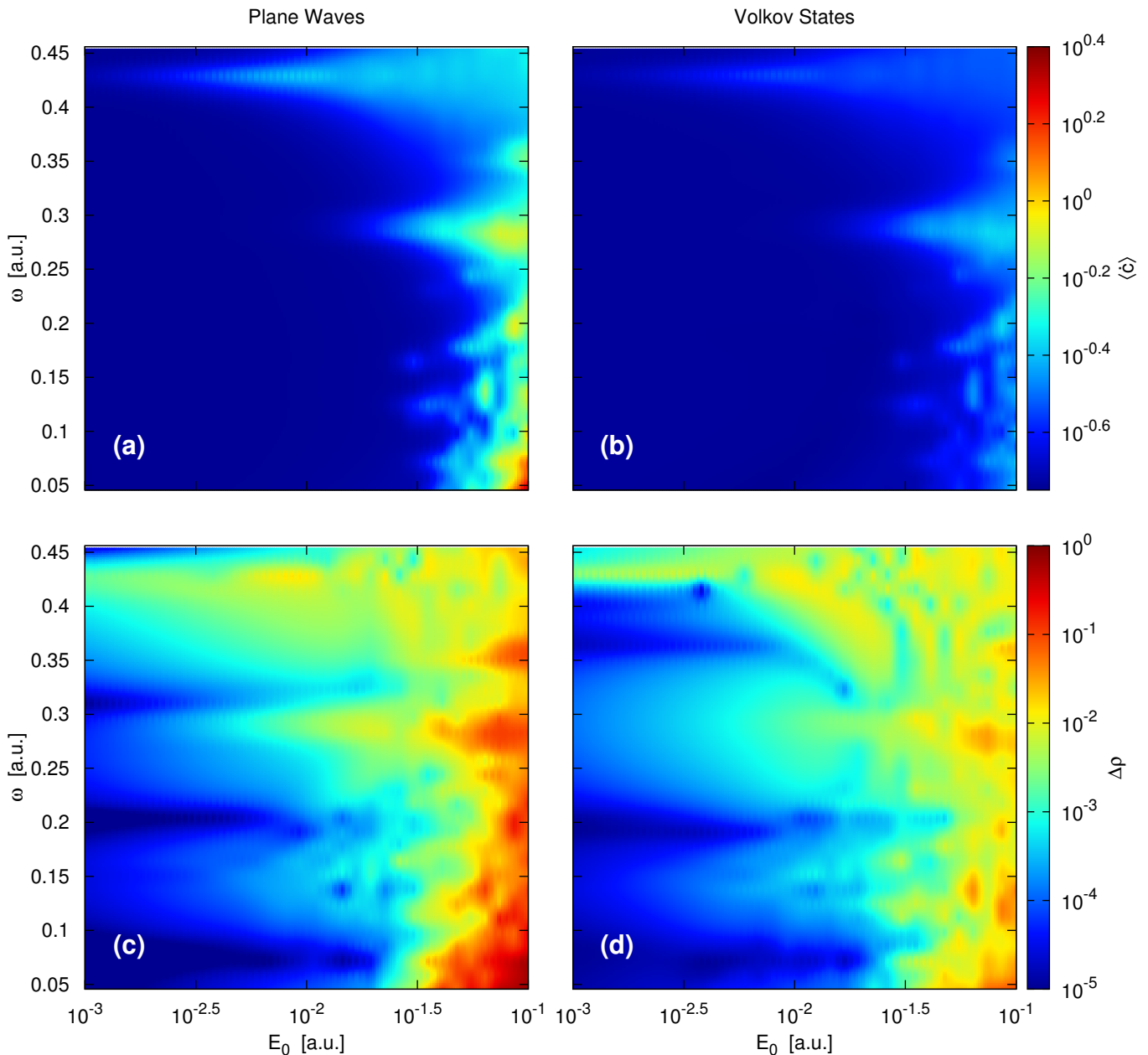


FIG. 2. (a,b) Time-averaged, k -integrated expansion coefficients and (c,d) density difference for both plane wave and Volkov state representations over a range of laser frequencies and amplitudes. The influence of the static Mathieu potential results in resonances corresponding to the $E_0 \rightarrow E_1$ and $E_1 \rightarrow E_2$ transitions at 0.428 a.u. and 0.154 a.u., respectively, and the $E_0 \rightarrow E_2$ double photon transition at 0.291 a.u. In plots (a) and (b), a time step size of 0.005 a.u. has been used, while plots (c) and (d) show the density difference between runs using 0.05 a.u. and 0.005 a.u.

to the fact that, in this region, the solution approaches being analytically described by this representation. Similarly, for the plane wave representation, higher frequency fields are easier to describe as the additional complexity of including a perturbation is minimized. For both cases, higher field strengths result in more oscillatory expansion coefficients indicating a heightened difficulty when attempting to propagate the wave function. Most importantly, the Volkov state coefficients are seen to vary significantly more smoothly overall which speaks to that

representation's advantage.

Instead, via inductive reasoning, one may also assess the two representations by comparing the resulting final densities, $\rho(x) = |\psi(x, t_{\text{final}})|^2$, of large time step simulations to the small time step, converged solutions by the metric $\Delta\rho \equiv \int |\rho_{\text{converged}}(x) - \rho(x)| dx$. These results are presented in Figs. 2c and 2d for the same range of field strengths and frequencies and provide a more straightforward depiction of the Volkov state expansion's ability to better represent laser-induced dynamics. The trends

match those found by analyzing the average change in coefficients. We conclude that the advantage of the Volkov state basis is best realized for field strengths above ~ 0.3 a.u., corresponding to ~ 1.5 V/Å or, equivalently, an intensity of $\sim 3.0 \times 10^{13}$ W/cm².

Next, we present results for the real-time TDDFT propagation of laser excited diamond using the Volkov state basis for a variety of laser intensities and frequencies. For this case, we solve the time-dependent Kohn–Sham equation

$$i \frac{\partial \phi_k(\mathbf{r}, t)}{\partial t} = \left[\frac{1}{2} [-i\nabla + \mathbf{A}(t)]^2 + V^{\text{KS}}[\rho](\mathbf{r}) \right] \phi_k(\mathbf{r}, t), \quad (18)$$

where

$$V^{\text{KS}}[\rho](\mathbf{r}) = V^{\text{H}}[\rho](\mathbf{r}) + V^{\text{XC}}[\rho](\mathbf{r}) + V^{\text{ion}}(\mathbf{r}). \quad (19)$$

Here, V^{H} is the Hartree potential,

$$V^{\text{H}}[\rho](\mathbf{r}) = \int \frac{\rho(\mathbf{r}')}{|\mathbf{r} - \mathbf{r}'|} d\mathbf{r}', \quad (20)$$

V^{XC} is the exchange–correlation potential, described in this work by the adiabatic local density approximation, and V^{ion} represents the potential due to the nuclei and core electrons, described using norm-conserving Troullier and Martins pseudopotentials [18]. In each simulation, the vector potential is simultaneously propagated via the Verlet algorithm as explained in Ref. 19. The external vector potential was evaluated at each time step using the analytical integral of the electric field, Eq. (17), which was defined using a squared sine envelope with pulse length T :

$$\mathbf{E}(t) = \mathbf{E}_0 \sin\left(\frac{\pi t}{T}\right)^2 \sin(\omega t). \quad (21)$$

The results were compared to benchmark real-space grid calculations employing a Taylor expansion for the discrete time step propagator, Eq. (14). Note that the upper limit of the time step in Taylor propagation is about $\Delta t = 0.005$ a.u.—larger time steps make the approach unstable. Other time propagation approaches, e.g. Crank–Nicolson, are prohibitively expensive in grid based approaches. The Volkov state basis propagation, in each of the following simulations, was employed via the split operator description discussed in Ref. 20. The potential exponential was split in order to treat the non-local pseudopotential term in the fashion described by Ref. 21.

For each Volkov state basis simulation, the initial state was prepared self-consistently using conjugate gradient method for the plane wave basis Kohn–Sham Hamiltonian, as opposed to converging the ground state using a real-space finite difference approach and Fourier transforming to a plane wave basis once finished. This detail is important as the nonlinearity of the Kohn–Sham equations leads to enhanced sensitivity to the choice of initial

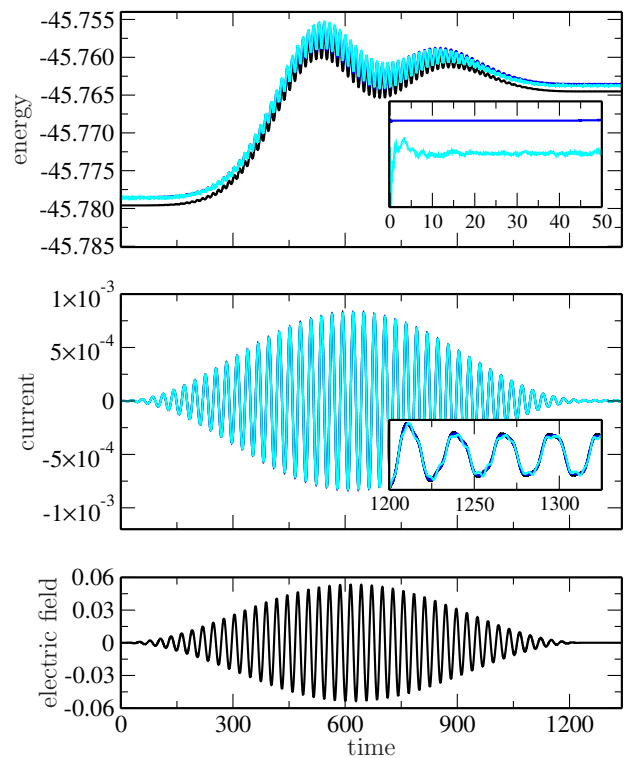


FIG. 3. Energy and current results for real-space grid and Volkov state bases corresponding to laser energy 6.05 eV, intensity 1×10^{14} W/cm², and width 30 fs. The real-space grid representation has been propagated using the Taylor expansion of the discrete time step propagator and a time step size of 0.005 a.u. (black). Volkov state basis results are shown for time step sizes of 0.005 a.u. (blue) and 0.05 a.u. (cyan). Insets highlight oscillation in early energies and later currents for Volkov propagations. These calculations were performed using an $8 \times 8 \times 8$ \mathbf{k} -point mesh.

state, and by preparing our system in this manner, we avoid a small perturbation at $t = 0$ attributed to the two different representations of the kinetic energy operator.

In the example calculation, we choose a high intensity laser, $I > 3 \times 10^{13}$ W/cm², because in this regime one expects the Volkov state basis propagation to display significant accuracy improvement as compared to full Hamiltonian discrete time step propagation methods. In the case of intense lasers applied to systems using pseudopotentials to describe frozen core electrons, the upper bound on the range of considered intensities should be around 10^{15} W/cm² [22]. In the following tests, the diamond unit cell is impacted by a laser pulse of intensity 1×10^{14} W/cm².

The Volkov state propagated energy and current, shown in Fig. 3, behave well for large time step sizes. The results for both 0.005 a.u. and 0.05 a.u. time step sizes nearly overlap. While the overall features of these results are well represented by the Volkov propagation, one notices the effect of nonlinear elements occurring in the Hamiltonian, namely the Hartree and exchange–correlation potentials. These terms lead to unavoidable

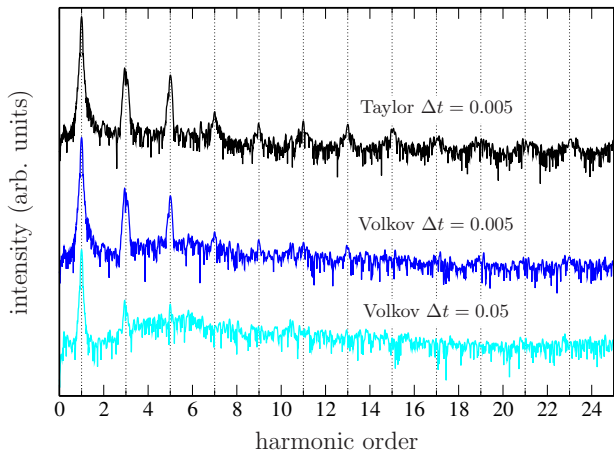


FIG. 4. High harmonic generation results for both real-space grid and Volkov state bases corresponding to the current results shown in Fig. 3. The employed window function is the pulse envelope.

small oscillations in the early energy. While these non-physical features cannot be completely eliminated, they are significantly diminished by choosing a smaller time step size, see the energy inset of Fig. 3. These oscillations lead to growing noise in the resulting current, shown in the current inset of Fig. 3.

Here, the increased magnitude of the current lessens the impact of the oscillations related to the Volkov state basis propagation. Figure 4 shows the spectral response in which the first few harmonic resonance peaks are pronounced. Even when using a time step size of 0.05, the Volkov state basis propagation is capable of distinguishing modes related to the third and fifth harmonics. This example illustrates that for high intensities, the Volkov state basis representation is capable of accurately describing complex electron density dynamics using time step sizes roughly an order of magnitude greater than that of the real-space Taylor propagation method.

It is important to note that the Volkov potential matrix elements are easily related to the plane wave potential matrix elements by the relation

$$V_{\mathbf{k}\mathbf{k}'}^V = V_{\mathbf{k}\mathbf{k}'}^{\text{PW}} e^{i(\Phi^{\mathbf{k}} - \Phi^{\mathbf{k}'})}, \quad (22)$$

where $V_{\mathbf{k}\mathbf{k}'}^{\text{PW}}(t)$ represents $\langle \phi_{\mathbf{k}}^{\text{PW}} | V(t) | \phi_{\mathbf{k}'}^{\text{PW}} \rangle$ and does not carry any direct contributions from the vector potential. This representation makes clear the simplicity of calculating Volkov state matrix elements. One may transform existing plane wave basis programs into Volkov state basis programs in a straightforward manner by calculating the Volkov phase difference via integration of the vector potential and applying the resulting phase factor to existing plane wave potential matrix elements which are readily available and employed in many popular codes—examples include VASP [23], ABINIT [24], and QUANTUM ESPRESSO [25]. Furthermore, due to the fact that this Volkov phase difference equals zero at $t = 0$, one may calculate the time-independent field-free ground state by use of existing plane wave basis methods. Note, however, that plane wave codes typically cut off the plane waves above a preset kinetic energy value in order to suppress the basis dimension. In time-dependent calculations of systems subjected to strong laser pulses, the inclusion of high kinetic energy plane waves may be necessary.

In conclusion, the Volkov state basis was implemented and tested for representing periodic structures in both one- and three-dimensional cases against the plane wave basis and real-space grid representations, respectively. In either scenario, the Volkov state basis propagation was capable of besting the conventional methods by allowing for a significant increase in time step size when describing interactions with fields of intensity greater than 3×10^{13} W/cm². For the case of representing bulk diamond, the Volkov state basis propagation successfully produced current oscillation modes related to the third and fifth harmonics, even at large time step sizes. This approach may be easily implemented within existing plane wave codes by the straightforward calculation of the time-dependent Volkov phase factors.

This work was supported by the National Science Foundation (NSF) under Grants No. Phy 1314463 and No. IIA126117. This work used the Extreme Science and Engineering Discovery Environment (XSEDE), which is supported by NSF grant No. ACI-1053575.

[1] F. Krausz and M. Ivanov, *Rev. Mod. Phys.* **81**, 163 (2009).
 [2] M. F. Ciappina, J. A. Prez-Hernandez, A. S. Landsman, W. A. Okell, S. Zherebtsov, B. Frg, J. Schtz, L. Seifert, T. Fennel, T. Shaaran, T. Zimmermann, A. Chacn, R. Guichard, A. Zair, J. W. G. Tisch, J. P. Marangos, T. Witting, A. Braun, S. A. Maier, L. Roso, M. Krger, P. Hommelhoff, M. F. Kling, F. Krausz, and M. Lewenstein, *Rep. Prog. Phys.* **80**, 054401 (2017).
 [3] S. Baker, I. A. Walmsley, J. W. G. Tisch, and J. P. Marangos, *Nat. Photonics* **5**, 665 (2011).

[4] S.-W. Huang, G. Cirimi, J. Moses, K.-H. Hong, S. Bhardwaj, J. R. Birge, L.-J. Chen, E. Li, B. J. Eggleton, G. Cerullo, and F. X. Kärtner, *Nat. Photonics* **5**, 475 (2011).
 [5] T. Tamaya, A. Ishikawa, T. Ogawa, and K. Tanaka, *Phys. Rev. Lett.* **116**, 016601 (2016).
 [6] T. Higuchi, M. I. Stockman, and P. Hommelhoff, *Phys. Rev. Lett.* **113**, 213901 (2014).
 [7] A. L. Cavalieri, N. Muller, T. Uphues, V. S. Yakovlev, A. Baltuska, B. Horvath, B. Schmidt, L. Blumel, R. Holzwarth, S. Hendel, M. Drescher, U. Kleineberg,

- P. M. Echenique, R. Kienberger, F. Krausz, and U. Heinzmann, *Nature* **449**, 1029 (2007).
- [8] P. Fldi, M. G. Benedict, and V. S. Yakovlev, *New J. Phys.* **15**, 063019 (2013).
- [9] M. S. Wismer, S. Y. Kruchinin, M. Ciappina, M. I. Stockman, and V. S. Yakovlev, *Phys. Rev. Lett.* **116**, 197401 (2016).
- [10] D. Golde, T. Meier, and S. W. Koch, *Phys. Rev. B* **77**, 075330 (2008).
- [11] E. Runge and E. K. U. Gross, *Phys. Rev. Lett.* **52**, 997 (1984).
- [12] K. Yabana, T. Sugiyama, Y. Shinohara, T. Otobe, and G. F. Bertsch, *Phys. Rev. B* **85**, 045134 (2012).
- [13] T. Otobe, Y. Shinohara, S. A. Sato, and K. Yabana, *Phys. Rev. B* **93**, 045124 (2016).
- [14] S. A. Sato, Y. Shinohara, T. Otobe, and K. Yabana, *Phys. Rev. B* **90**, 174303 (2014).
- [15] G. Wächter, C. Lemell, J. Burgdörfer, S. A. Sato, X.-M. Tong, and K. Yabana, *Phys. Rev. Lett.* **113**, 087401 (2014).
- [16] N. Tancogne-Dejean, O. D. Mücke, F. X. Kärtner, and A. Rubio, *Phys. Rev. Lett.* **118**, 087403 (2017).
- [17] X. Zhang, F. Wang, L. Jiang, and Y. Yao, *Phys. Rev. B* **95**, 184301 (2017).
- [18] N. Troullier and J. L. Martins, *Phys. Rev. B* **43**, 1993 (1991).
- [19] Y. Li, S. He, A. Russakoff, and K. Varga, *Phys. Rev. E* **94**, 023314 (2016).
- [20] C. Covington, D. Kidd, J. Gilmer, and K. Varga, *Phys. Rev. A* **95**, 013414 (2017).
- [21] O. Sugino and Y. Miyamoto, *Phys. Rev. B* **59**, 2579 (1999).
- [22] X.-M. Tong, G. Wächter, S. A. Sato, C. Lemell, K. Yabana, and J. Burgdörfer, *Phys. Rev. A* **92**, 043422 (2015).
- [23] G. Kresse and J. Furthmüller, *Phys. Rev. B* **54**, 11169 (1996).
- [24] X. Gonze, F. Jollet, F. Araujo, D. Adams, B. Amadon, T. Applencourt, C. Audouze, J.-M. Beuken, J. Bieder, A. Bokhanchuk, E. Bousquet, F. Bruneval, D. Caliste, M. Cote, F. Dahm, F. Pieve, M. Delaveau, M. G. ando B. Dorado, C. Espejo, G. Geneste, L. Genovese, A. Gerossier, M. Giantomassi, Y. Gillet, D. R. Hamann, L. He, G. Jomard, J. Janssen, S. Roux, A. Levitt, A. Lherbier, F. Liu, I. Lukacevic, A. Martin, C. Martins, M. J. T. Oliveira, S. Ponce, Y. Pouillon, T. Rangel, G.-M. Rignanese, A. H. Romero, B. Rousseau, O. Rubel, A. A. Shukri, M. Stankovski, M. Torrent, M. Setten, B. Troeye, M. J. Verstraete, D. Waroquier, J. Wiktor, B. Xue, A. Zhou, and J. W. Zwanziger, *Comput. Phys. Commun.* **205**, 106 (2016).
- [25] P. Giannozzi, S. Baroni, N. Bonini, M. Calandra, R. Car, C. Cavazzoni, D. Ceresoli, G. L. Chiarotti, M. Cococcioni, I. Dabo, A. Dal Corso, S. de Gironcoli, S. Fabris, G. Fratesi, R. Gebauer, U. Gerstmann, C. Gougoussis, A. Kokalj, M. Lazzeri, L. Martin-Samos, N. Marzari, F. Mauri, R. Mazzarello, S. Paolini, A. Pasquarello, L. Paulatto, C. Sbraccia, S. Scandolo, G. Sclauzero, A. P. Seitsonen, A. Smogunov, P. Umari, and R. M. Wentzcovitch, *J. Phys. Condens. Matter* **21**, 395502 (19pp) (2009).